
A MACHINE-LEARNED EXPRESSION FOR THE EXCESS GIBBS ENERGY

Marco Hoffmann[†]

Laboratory of Engineering Thermodynamics
RPTU Kaiserslautern, Germany
marco.hoffmann@rptu.de

Thomas Specht[†]

Laboratory of Engineering Thermodynamics
RPTU Kaiserslautern, Germany
thomas.specht@rptu.de

Quirin Göttl

Laboratory of Chemical Process Engineering
Technical University of Munich, Germany
qgctvtum@gmail.com

Jakob Burger

Laboratory of Chemical Process Engineering
Technical University of Munich, Germany
burger@tum.de

Stephan Mandt

Department of Computer Science & Statistics
University of California, Irvine
mandt@uci.edu

Hans Hasse

Laboratory of Engineering Thermodynamics
RPTU Kaiserslautern, Germany
hans.hasse@rptu.de

Fabian Jirasek*

Laboratory of Engineering Thermodynamics
RPTU Kaiserslautern, Germany
fabian.jirasek@rptu.de

ABSTRACT

The excess Gibbs energy plays a central role in chemical engineering and chemistry, providing a basis for modeling the thermodynamic properties of liquid mixtures. Predicting the excess Gibbs energy of multi-component mixtures solely from the molecular structures of their components is a long-standing challenge. In this work, we address this challenge by integrating physical laws as hard constraints within a flexible neural network. The resulting model, HANNA, was trained end-to-end on an extensive experimental dataset for binary mixtures from the Dortmund Data Bank, guaranteeing thermodynamically consistent predictions. A novel surrogate solver developed in this work enabled the inclusion of liquid-liquid equilibrium data in the training process. Furthermore, a geometric projection method was applied to enable robust extrapolations to multi-component mixtures, without requiring additional parameters. We demonstrate that HANNA delivers excellent predictions, clearly outperforming state-of-the-art benchmark methods in accuracy and scope. The trained model and corresponding code are openly available, and an interactive interface is provided on our website, MLPROP.

*Corresponding author

[†]These authors contributed equally.

1 Main

Accurate knowledge of the thermodynamic properties of liquid mixtures is crucial in chemistry, chemical engineering, and environmental science. Among these properties, the molar excess Gibbs energy, g^E , plays a central role: it provides the foundation for deriving many other thermodynamic quantities through established relations. In particular, g^E serves as the basis for determining the activity coefficients of the mixture’s components.

Activity coefficients, in turn, govern phase equilibria, such as vapor-liquid (VLE), liquid-liquid (LLE), and solid-liquid (SLE) equilibria, and are key to describing chemical equilibria. They are also used in modeling reaction kinetics, and transport phenomena. This makes g^E a central property in model-based process design and optimization. However, g^E and the derived activity coefficients cannot be measured directly but must be inferred from phase equilibrium data, and the corresponding experiments are costly and time-consuming.

Given the many thousands of technically relevant components that can form an enormous number of mixtures, and the fact that g^E depends on the state point (especially temperature and composition in liquid mixtures), only a tiny fraction of all relevant mixtures can be studied experimentally. This makes the development of predictive models for g^E a central task in thermodynamics. We thereby distinguish different classes of predictions, namely, to:

- *Unstudied state points*: temperatures and/or compositions of a mixture for which data exist at other conditions.
- *Unstudied systems*: combinations of components for which data exist in other systems.
- *Unstudied components*: entirely new substances for which no data exist.

All common g^E -models are based on the concept of pair interactions. The most widely used g^E -models are lattice models, such as NRTL [1] and UNIQUAC [2], in which the molecular interactions are described by pair-interaction parameters between components, which are usually fitted to experimental data for each binary system of interest. These models enable predictions for unstudied temperatures and compositions, as well as predictions for multi-component mixtures, if data exists to fit the model parameters of all constituent binary subsystems. However, these models do not allow predictions for unstudied components, binary systems, and multi-component mixtures comprising unstudied binary subsystems. Furthermore, these models suffer from limited flexibility, which often hinders the simultaneous description of VLE and LLE with a single parameterization [3, 4].

To address the lacking capability of predictions to unstudied systems and components, group-contribution (GC) g^E -models have been developed, with the different variants of UNIFAC being the most successful ones [5, 6, 7, 8]. UNIFAC decomposes components into structural groups and utilizes parameters that describe pair interactions between these groups, significantly reducing the number of parameters and enabling extrapolations to unstudied systems and components. However, UNIFAC is limited to mixtures for which all involved structural groups (and their interactions) have previously been parametrized. Furthermore, since UNIFAC is unable to describe both VLE and LLE with high accuracy, a special UNIFAC parameterization for LLE has been introduced [9]. Additionally, for describing complex systems, such as those containing ionic liquids [10, 11] or formaldehyde [12, 13], tailored groups had to be introduced, compromising the GC nature of UNIFAC and the generality of the approach. Despite the described shortcomings, the different UNIFAC variants have long been and remain the standard g^E -models used for phase equilibrium calculations in process simulations across industry and academia.

An alternative to the GC models of the UNIFAC family are the g^E -models from the COSMO family, in which the energetic contribution to g^E is calculated using COSMO methods from quantum chemistry [14], avoiding the need for group-interaction parameter tables. Several variants of COSMO-based g^E -models have been developed [15, 16, 17, 18], which will be referred to as COSMO models for brevity in the following. These models are based on quantum-chemical calculations of the individual components of the mixture embedded in an ideal conductor. These quantum-chemical calculations are feasible for most molecules; however, they are associated with considerable effort, and challenges regarding the treatment of conformers arise, with the results depending on the level chosen for the quantum-chemical calculation [17, 19, 20, 21]. While the COSMO models have a larger scope than UNIFAC, the predictions of UNIFAC are often found to be more accurate than those of COSMO for systems for which both methods can be applied [17, 22, 23].

Recently, several authors used machine learning (ML) methods to further extend the scope of the classical g^E -models by predicting their pair-interaction parameters. This was done for UNIQUAC [24], NRTL [25], and UNIFAC [26, 27]. These new hybrid methods rely on the underlying g^E -models and are therefore intrinsically physically consistent. However, these models also inherit all the limitations of the underlying g^E -models, e.g., the problems of simultaneously describing VLE and LLE, or the restriction to a predefined list of structural groups [26, 27] or components [24]. The SPT-NRTL model [25] is, in principle, applicable to arbitrary mixtures (although the limitations to simultaneously describe VLE and LLE still hold), but it is not openly available.

To overcome all described limitations, we present the first ML-based g^E -model that does not build on an existing physical model, but instead combines the flexibility of artificial neural networks with explicit physical knowledge hard-coded into the network architecture. This model, called HANNA (hard-constraint neural network for consistent activity coefficient prediction), builds on a prototype from our recent work [28], which was restricted to modeling VLE in binary systems. In this work, a generalization of HANNA is presented that is flexible enough for the holistic description of different phase equilibria (namely VLE and LLE), enables predictions for arbitrary components, binary and multi-component systems, and state points, and strictly complies with all relevant physical laws and constraints. The only input required for HANNA is the molecular structure of the components and the considered state point (temperature, composition). We provide the trained HANNA model to the scientific community open-source and also make it available through an intuitive user interface on our website MLPROP. Fig. 1 gives a high-level overview of HANNA and its training procedure.

The network structure of HANNA includes permutation-invariant operations, ensuring predictions are independent of the order of the components in the input, as well as operations that guarantee consistency in the limiting cases of the binary subsystems and pure components. To generalize to multi-component mixtures, we introduce a geometric projection method [31] that maps the g_{ij}^E of the binary subsystems into the multi-component space. Because this projection does not introduce additional parameters, it is sufficient to train the model only on data of binary mixtures. Furthermore, the projection strictly fulfills all consistency criteria regarding the extrapolation to multi-component

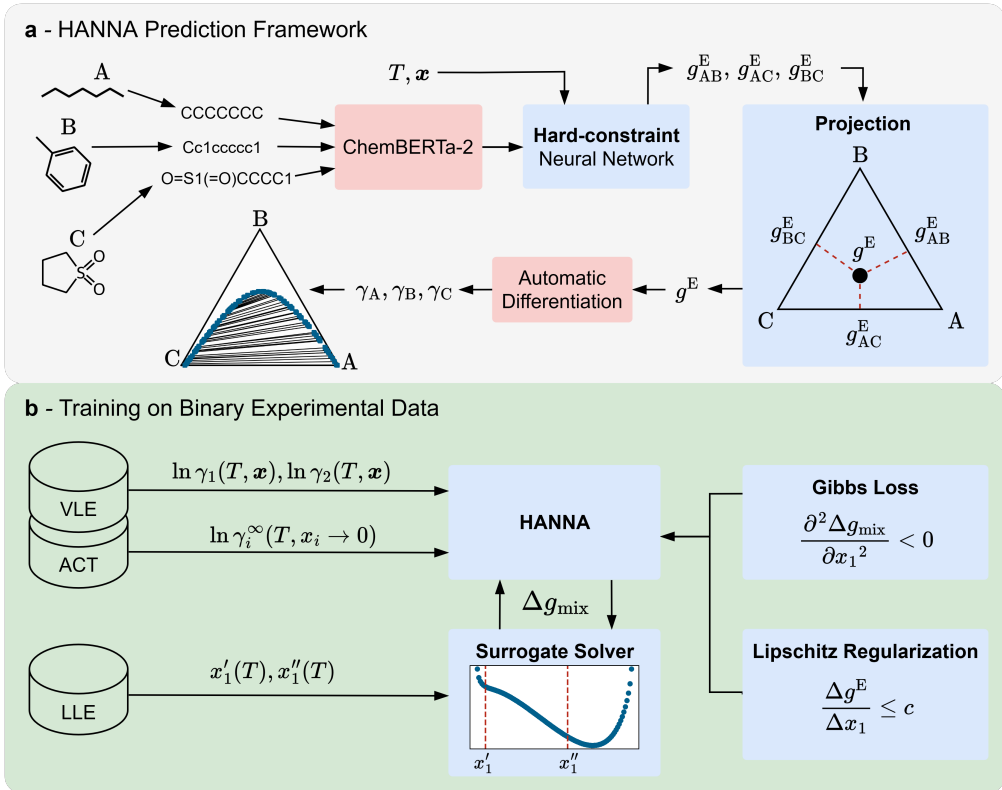


Figure 1: Overview of the HANNA prediction framework (for a ternary mixture as illustrative example) and its training procedure. **a**, As input, HANNA requires the molecular structure of all components in the SMILES [29] notation, the composition of the mixture \mathbf{x} , and the temperature T . In the first step, molecular embeddings are generated from the SMILES using the transformer model ChemBERTa-2 [30]. Subsequently, a hard-constraint neural network that strictly obeys all thermodynamic constraints predicts g_{ij}^E of all binary subsystems, from which g^E in the multi-component mixture is calculated via a geometric projection [31]. Thermodynamically consistent activity coefficients γ_i are obtained by automatic differentiation of g^E and then used to predict phase equilibria using the convex envelope method (CEM) [32, 33, 34]. **b**, HANNA is trained on the activity coefficients derived from binary VLE data, activity coefficients at infinite dilution (ACI) data, and the phase compositions x'_1, x''_1 from LLE data. End-to-end training on the experimental LLE data is enabled by a new surrogate solver using the molar Gibbs energy of mixing Δg_{mix} . An additional Gibbs loss incentivizes the model to produce negative second derivatives of Δg_{mix} in the LLE regime, and a Lipschitz regularization enforces smoother g^E functions.

mixtures. The projection approach is generic and can also be applied to other types of ML-based g^E -models that are currently limited to predicting binary mixtures. Details on the HANNA architecture and the projection are given in Section 4.1.

HANNA was trained end-to-end on extensive experimental data sets of binary mixtures, including activity coefficients (normalized after Raoult’s law) derived from vapor-liquid equilibria (VLE) and infinite dilution activity coefficients (ACI), as well as phase compositions of liquid-liquid equilibria (LLE) from the Dortmund Data Bank [35]. The data set covers 337,276 data points (95 % of them between 273 and 433 K) in 36,437 unique systems of 3079 unique components with a large chemical diversity, also including ionic liquids. Details on the data sets can be found in Section 4.2. To incorporate the LLE data into the training process, we developed a new training strategy based on a surrogate solver that circumvents the necessity for iteratively solving non-linear equations during training [36]. To the best of our knowledge, this is the first time that experimental phase compositions from LLE data were used in the end-to-end training of a ML-based g^E -model. We also introduce a physically inspired ‘Gibbs loss’ that enhances the recognition and description of LLE based on the stability criterion [36]. Additionally, a Lipschitz regularization strategy was employed, which increases the robustness of HANNA in regions outside the training regime by enforcing the smoothness of the predicted g^E . Details on the model training are given in Section 4.4.

HANNA is the first publicly available ML-based g^E -model that applies to multi-component mixtures of arbitrary components and can correctly predict different phase equilibria with a single parameterization. To demonstrate the performance of HANNA, we consider the prediction of VLE and LLE in binary and ternary mixtures in the following. Detailed results for quaternary systems are provided in the Supporting Information. The results presented here were obtained exclusively on unseen test systems that were withheld during the training process of HANNA.

2 Results and Discussion

2.1 Predictions for Binary Mixtures

Figure 2 compares HANNA’s predictive performance for binary mixtures against that of modified UNIFAC (Dortmund) [7, 8], hereafter referred to as mod. UNIFAC.

We use mod. UNIFAC as the primary benchmark in this work, because it is the most established g^E -model in industry and academia. Additionally, we compare HANNA to mod. UNIFAC 2.0 [27], a ML-enhanced version of UNIFAC that exceeds the original model in scope due to a completed interaction parameter matrix. Furthermore, we also compare HANNA to UNIFAC-LLE [9], a version of UNIFAC that was specifically parameterized to describe LLE data between 283.15 K and 313.15 K. The comparisons to mod. UNIFAC 2.0 and UNIFAC-LLE on binary mixtures can be found in the Supporting Information (cf. Figs. S.8 and S.11, respectively). HANNA surpasses both models in scope and accuracy.

The results shown in the boxplots of Fig. 2a demonstrate that HANNA outperforms mod. UNIFAC in prediction accuracy on the shared mod. UNIFAC horizon (i.e., all systems to which mod. UNIFAC could be applied) for all studied data types: vapor-liquid equilibria (VLE, top), activity coefficients at infinite dilution (ACI, middle), and liquid-liquid equilibrium (LLE, bottom). We assess the performance using the system-specific mean absolute error MAE_{sys} , cf. Section 4.5. The most significant difference is found for the ACI data, where the median of the system-specific mean absolute error MAE_{sys} is halved from 0.2 (mod. UNIFAC) to 0.1 (HANNA). This significant difference could be related to a deficiency of UNIFAC (on which UNIFAC is based) to correctly predict infinite dilution activity coefficients in strongly non-ideal systems [37].

Beyond the mod. UNIFAC horizon, the performance of HANNA slightly declines for the VLE and LLE data (cf. full horizon), which could be attributed to systems with complex components containing rarely occurring groups that mod. UNIFAC fails to predict entirely because not enough data were available to regress the required parameters. Importantly, for the LLE data, error scores could only be calculated if the respective model predicts a miscibility gap at the given state point. Therefore, the number of systems for which predictions are obtained differs from the number of systems within the LLE data set that are theoretically feasible with the models. On the mod. UNIFAC horizon, mod. UNIFAC correctly identifies miscibility gaps for 80 % of the LLE systems, whereas HANNA achieves 91 % accuracy. On the full horizon, HANNA correctly identifies miscibility gaps for 87 % of the LLE systems.

The full horizon of the ACI data on which we evaluate HANNA contains more than twice as many systems as the mod. UNIFAC horizon. The largest share of these additional systems contains at least one ionic liquid (IL). As only very few groups to model ILs have been parameterized within mod. UNIFAC, its scope regarding mixtures containing ILs is very limited. In contrast, HANNA does not have any restrictions concerning ILs. In Fig. S.7 in the Supporting Information, we evaluate the performance of HANNA for predicting activity coefficients in IL systems and compare it to that of

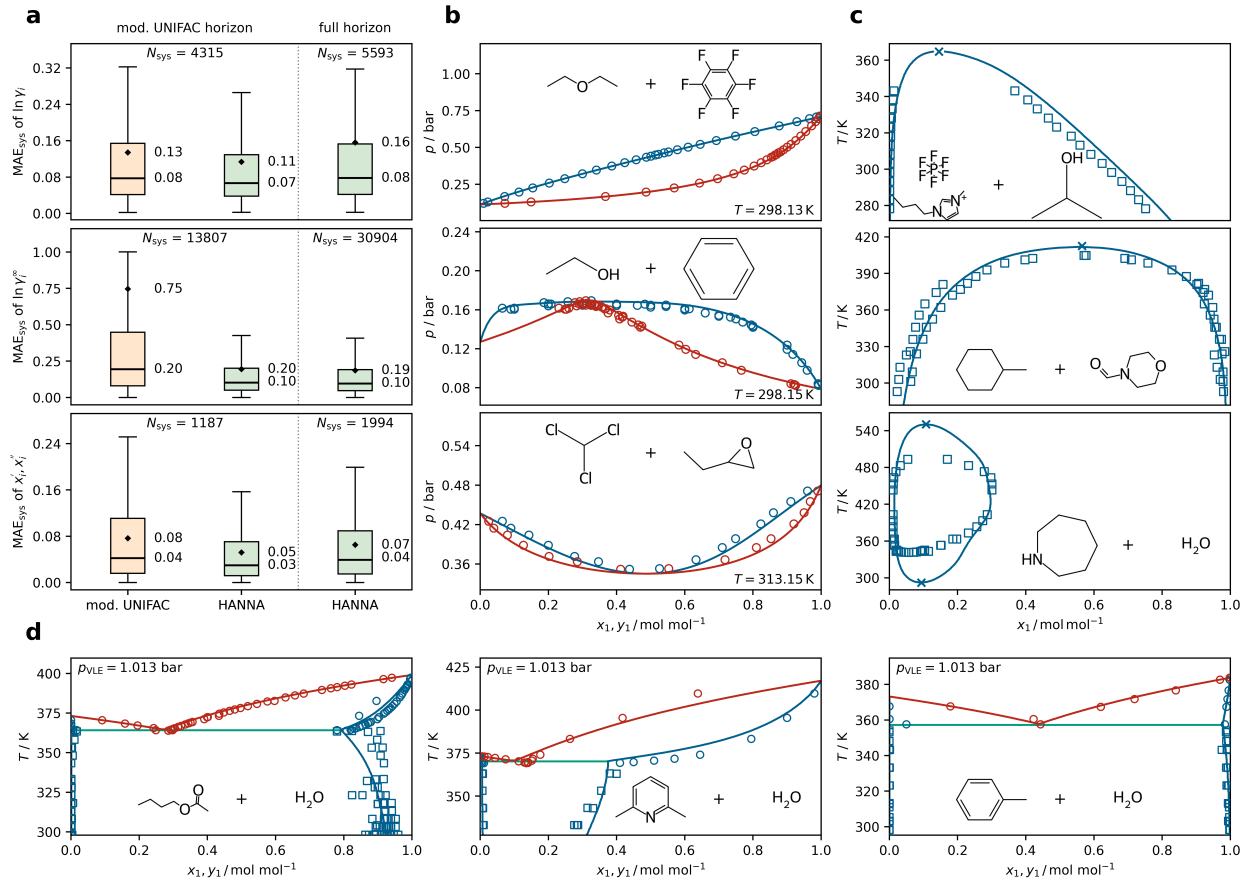


Figure 2: Predictions for binary mixtures with HANNA. **a**, Boxplots comparing the performance of HANNA for predicting activity coefficients in binary VLE (top), ACI (middle), and LLE phase compositions (bottom) with that of mod. UNIFAC in terms of the system-wise mean absolute error MAE_{sys} in γ_i (VLE, ACI) or phase compositions x'_i and x''_i (LLE). For a fair comparison, HANNA was also evaluated only on those systems for which mod. UNIFAC is applicable (mod. UNIFAC horizon). N_{sys} denotes the number of test systems within the respective horizon and data type. The boxes represent interquartile ranges and the whiskers are 1.5 times the interquartile range. Diamonds mark the mean, horizontal lines the median of the MAE_{sys} values. **b**, Predictions of HANNA for three isothermal VLE plotted against experimental data. Open symbols denote experimental data, lines are predictions by HANNA. Blue color marks the liquid phase; red color marks the vapor phase. Molecular structures of the components are depicted within the plots. The left molecule corresponds to component 1. **c**, Predictions of HANNA for three LLE. Open squares indicate experimental data, lines represent predictions by HANNA. Predicted upper and lower critical solution temperatures are marked with an 'x'. **d**, Predictions of HANNA for three isobaric heteroazeotropes. Open blue and red circles indicate the experimental liquid and vapor phases, respectively, from VLE data. Open blue squares mark the experimental phase compositions from LLE data; the green line is the vapor-liquid-liquid equilibrium predicted by HANNA. All results shown here are for systems from the test set that were not included in the training of HANNA.

mod. UNIFAC for the few IL systems for which mod. UNIFAC can be used. The results show an excellent prediction accuracy of HANNA also for IL systems, again significantly outperforming mod. UNIFAC on the shared horizon.

Three typical examples for predictions of binary VLE diagrams with HANNA are shown in Fig. 2b. The predictions were obtained using extended Raoult's law with vapor pressures calculated from the Antoine parameters of the DDB [35]. For all systems, HANNA shows excellent agreement with experimental data. HANNA correctly describes nearly ideal mixtures (top), mixtures with strong negative (middle), and mixtures with strong positive (bottom) deviations from Raoult's law.

Fig. 2c demonstrates that HANNA can also successfully predict LLE phase diagrams. For the predictions, we assume a pressure-independent LLE. Even the island-type miscibility gap with an upper and a lower critical solution temperature

is correctly predicted (bottom). As for the ACI data, HANNA also yields good predictions for LLE involving ionic liquids (top).

In Fig. 2d, predictions of HANNA for three heteroazeotropic mixtures are shown. For each mixture, HANNA accurately captures the experimental phase behavior, demonstrating HANNA's applicability over a wide temperature range. Both VLE and LLE are predicted well, which is in sharp contrast to the commonly used g^E -models based on lattice theory, which struggle with this task. The diagrams in Figs. 2c and 2d were obtained using the convex envelope method (CEM) [32, 33, 34], which enables a seamless calculation of different types of phase equilibria, considering the global behavior of the studied mixture, and thus avoiding individual phase equilibrium calculations and the problems associated with this. In Fig. S.5 in the Supporting Information, we evaluate the predictions of mod. UNIFAC on the systems of Figs. 2b, 2c, and 2d that fall within the mod. UNIFAC horizon. The results emphasize the superior predictive power of HANNA.

2.2 Predictions for Ternary Mixtures

Figure 3 evaluates HANNA's performance on unseen ternary mixtures.

Similar to the results for the binary mixtures, Fig. 3a depicts boxplots of the system-wise MAE for the predictions of activity coefficients in ternary VLE (top), infinite dilution activity coefficients in mixed solvents (ACI, middle), and LLE (bottom), and compares the performance of HANNA to that of mod. UNIFAC. Again, we have also compared HANNA against mod. UNIFAC 2.0 and UNIFAC-LLE, which yielded similar results as those against mod. UNIFAC shown here (cf. Figs. S.9 and S.12 in the Supporting Information, respectively).

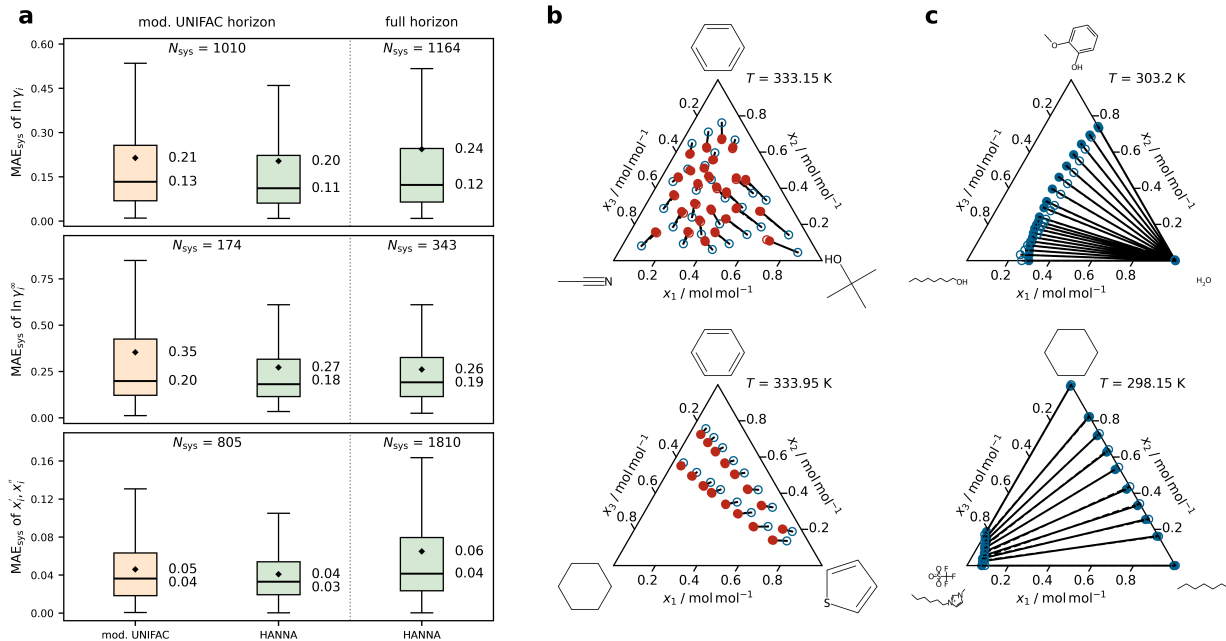


Figure 3: Predictions for ternary mixtures with HANNA. **a**, Boxplots comparing the performance of HANNA for predicting activity coefficients in ternary VLE (top), ACI (middle), and LLE phase compositions (bottom) with that of mod. UNIFAC in terms of the system-wise mean absolute error MAE_{sys} in γ_i (VLE, ACI) or phase compositions x'_i and x''_i (LLE). For a fair comparison, HANNA was also evaluated only on those systems for which mod. UNIFAC is applicable (mod. UNIFAC horizon). N_{sys} denotes the number of test systems within the respective horizon and data type. The boxes represent interquartile ranges and the whiskers are 1.5 times the interquartile range. Diamonds mark the mean, horizontal lines the median of the MAE_{sys} values. **b**, Predictions of HANNA for two isothermal VLE. Open blue and red symbols mark the experimental liquid and vapor phase compositions, respectively; filled red symbols are the vapor phase compositions. Molecular structures represent the respective pure components. **c**, Predictions of HANNA for three isothermal LLE. Open symbols and dashed tie lines represent the experimental data; filled symbols and solid lines represent predictions by HANNA. All results shown here are for systems from the test set that were not included in the training of HANNA.

As for the binary data, HANNA shows higher accuracy than mod. UNIFAC within the mod. UNIFAC horizon on all three data types. Again, we observe a slight decline in the accuracy of HANNA on the VLE and LLE data on the full horizon. On the mod. UNIFAC horizon, mod. UNIFAC correctly identifies the miscibility gaps for 80 % of the ternary LLE systems, whereas HANNA achieves 98 % accuracy. On the full horizon, HANNA correctly identifies the miscibility gaps for 94 % of the systems.

Fig. 3b and Fig. 3c show HANNA predictions for ternary systems exhibiting a VLE or LLE, respectively, and compare them to experimental data. For the LLE prediction, we again neglect the pressure dependence of g^E . In all cases, an excellent agreement is found (in many cases, the open symbols denoting the experimental data are hidden by the closed symbols of the HANNA predictions).

Comparing HANNA’s performance on binary and ternary mixtures reveals how different extrapolation strategies influence accuracy across VLE, LLE, and ACI data (cf. panels **a** in Figs. 2 and 3). For the ternary VLE data, the scores from HANNA and mod. UNIFAC become slightly worse by the same margin (their median MAE_{sys} increases about 0.04), when compared to the respective binary scores. Considering the LLE data, when going from binary to ternary data, the scores remain almost constant for both methods. For the ACI data, we observe a significant deterioration of the predictions going from binary to ternary systems for HANNA (the median MAE_{sys} increases by 0.08), while this is not the case for mod. UNIFAC.

The extrapolation from binary to multi-component data in the UNIFAC variants is based on the physical lattice model using the pair-interaction concept. In contrast, HANNA uses a purely geometric projection method. To determine if the projection method is responsible for the deterioration of HANNA for ternary ACI data, we carried out the following test: for all systems in the ternary VLE and ACI data sets, we predicted the corresponding activity coefficient curves of all binary subsystems at the respective temperatures using HANNA. We then fitted two component-specific physical g^E -models (UNIQUAC and NRTL, the first being the parent model of UNIFAC) to these predicted activity coefficients and used the resulting fitted parameters to predict the activity coefficients in the ternary systems. This procedure allows a comparison of only the extrapolations of the physical models (UNIQUAC/NRTL) to the geometric extrapolation of HANNA, starting from the exact same binary data. The results of this comparison are shown in Figs. S.14 and S.15 in the Supporting Information and indicate a similar or even slightly better accuracy using the geometric projection for ternary data compared to the extrapolation of the physical models. Hence, the geometric Muggianu projection method in the HANNA architecture generally appears to work reasonably well. However, this does not exclude that further improvements can be made on the geometric extrapolation, for which different suggestions exist in the literature [38, 39].

The presented results demonstrate that HANNA outperforms mod. UNIFAC, the most established model for predicting activity coefficients in industry and academia, not only in applicability (unlike mod. UNIFAC, HANNA can model basically any system if the molecular structure of the comprising components is known), but also in prediction accuracy for all considered data types (VLE, ACI, LLE) for both binary and ternary mixtures. This result is especially remarkable because we have evaluated HANNA on data from the DDB, the largest factual database for thermodynamic properties, which is managed essentially by the same group that has revised mod. UNIFAC over the last decades. Consequently, we must assume that mod. UNIFAC has been fitted to a significant part of our test data (although the concrete training data for mod. UNIFAC has not been fully disclosed). Similar arguments hold for mod. UNIFAC 2.0 and UNIFAC-LLE. In contrast, the results of HANNA have been obtained on test data, strictly withholding *all available data types* for the test systems during model training. Hence, most comparisons we have shown here are biased in favor of mod. UNIFAC.

Limitations

We have demonstrated that HANNA provides accurate predictions for activity coefficients in binary and ternary mixtures, and that phase equilibria calculated from these predictions agree well with experimental data. The training data used here consists of VLE, ACI, and LLE, with 95 % of the data in a temperature range between 273 K and 433 K. HANNA can also be used to predict activity coefficients outside this temperature range and for phase equilibria with supercritical components (using Henry’s law) or solid-liquid equilibria (SLE). However, HANNA’s performance on these additional types of phase equilibria and outside the described temperature range is yet to be evaluated. Furthermore, HANNA, like most g^E -models, neglects the pressure dependence of the liquid phase activity coefficients. While this is an excellent assumption for most engineering applications, it may break down at very high pressures. Also note that at high pressures, the Poynting correction should be taken into account when applying Raoult’s law for predicting VLE.

HANNA was trained on a large and diverse set of data and has learned to accurately predict activity coefficients for mixtures of components from many classes, including both small and large molecular components, as well as components containing exotic chemical groups. Also, weak electrolytes and ionic liquids were included in the training set and are therefore within the current scope of HANNA. However, data on polymers were not considered, so

HANNA should not be used for polymer systems (note that this is currently also not possible for technical reasons, as ChemBERTa-2 does not support the correct conversion of SMILES into embeddings for molecules consisting of more than 512 tokens [40, 30]). Furthermore, HANNA was not trained on data for solutions of strong electrolytes (except ionic liquids), so that HANNA should not be used for these systems.

In the extensive tests we have carried out, HANNA consistently gave activity coefficients that led to plausible phase behaviors. The only exception to this was a small fraction of the binary LLE systems containing methanol, for which we found that HANNA predicts an implausible phase behavior.[†] We speculate that the ChemBERTa-2 [30] tokenization for methanol (SMILES: 'CO') into 'C' (equivalent to the SMILES for methane) and 'O' (equivalent to the SMILES for water) results in a methanol embedding that cannot fully capture the molecule’s properties. In the future, this could be overcome by introducing a distinct token for methanol and/or water; a similar strategy was used in mod. UNIFAC, which has dedicated groups for methanol and water.

While the Lipschitz regularization promotes the smoothness of the HANNA predictions with respect to a variation of the inputs (components, temperature, and composition), too strong regularizations overly restrict the model’s flexibility and reduce its predictive performance, cf. Fig. S.4 in the Supporting Information for a systematic assessment. With the chosen regularization, HANNA in some cases exhibits small fluctuations of the predicted activity coefficients with respect to the composition. Because this only affects systems that are close to ideal mixtures, i.e., with very small activity coefficients, this does not compromise HANNA’s practical applicability.

3 Conclusions

This work presents HANNA, the first publicly available ML-based g^E -model that enables the thermodynamically consistent prediction of activity coefficients in liquid mixtures with an arbitrary number of components solely from the chemical formula of the constituent components. HANNA was trained on a large and diverse set of thermodynamic data from measurements of vapor-liquid equilibria, activity coefficients at infinite dilution, and liquid-liquid equilibria, which gives it unprecedented applicability.

The results of HANNA were systematically compared to those from state-of-the-art models from the UNIFAC family for binary and ternary mixtures, demonstrating a superior performance of HANNA - despite an important bias of the comparison in favor of UNIFAC: while all results for HANNA were true predictions (none of the systems in our test set was used for training of HANNA), this is not true for UNIFAC, for which many of the systems in the test set were also used for the training. Even more importantly, HANNA has a much broader applicability than UNIFAC, and HANNA retains its accuracy for systems that cannot be described with UNIFAC.

HANNA is the first g^E -model in which the entire relevant physical knowledge is embedded in a neural network as hard constraints. It therefore fully leverages the flexibility of neural networks, but applies it only within the bounds permitted by physical principles. This flexibility enables HANNA to simultaneously describe vapor-liquid equilibrium data and liquid-liquid equilibrium data with high accuracy with a single parameterization, thereby overcoming the deficiencies of benchmark g^E -models.

A ready-to-use version of HANNA, trained on all available data for binary mixtures (including the data that were retained as test data for the comparison of the present work), is provided on GitHub. Furthermore, we also provide an interactive interface for HANNA on our website MLPROP. We encourage users to give us feedback.

Several enabling technologies used within the work on HANNA merit to be highlighted, as they are useful far beyond the work described here: 1) Based on the convex envelope method (CEM), we have developed a new surrogate solver for determining LLE phase compositions that can be incorporated in the workflow of ML model training. 2) By applying a geometric projection method, a model for predicting properties of binary mixtures can be seamlessly extended to multi-component mixtures without the need for additional parameters. 3) Using the CEM for determining phase equilibria, we have overcome limitations of conventional phase equilibrium solvers and were able to robustly predict phase equilibria of different types for thousands of systems in an automated way.

HANNA represents a major advancement in predicting the thermodynamic properties of liquid mixtures. It will improve process design and optimization, and ease their application. Additionally, HANNA is highly interesting for material design, e.g., for identifying promising solvents for chemical reactions and separation processes like extraction, extractive distillation, absorption, and crystallization.

[†]Specifically, it predicts the existence of two separate LLE phase regions for one temperature, which is thermodynamically possible, but, to the best of our knowledge, not experimentally found for these systems.

Outlook

The current version of HANNA is already a widely applicable and accurate g^E -model that outperforms current state-of-the-art benchmark models. To further extend the scope of HANNA, future developments will address the following issues:

Database and methods. In this work, we have used data from measurements of vapor-liquid equilibria (VLE), activity coefficients at infinite dilution (ACI), and liquid-liquid equilibria (LLE) for training HANNA. In future work, data on solid-liquid equilibria (SLE), from which activity coefficients can be derived, could also be included. These data would extend the temperature range of the training data at its lower end. Furthermore, data on excess enthalpies h^E and excess heat capacities c_p^E could be used for the training. These properties can be obtained from the g^E -model by derivations with respect to temperature and are easily accessible within the HANNA framework by automatic differentiation. So far, only binary data have been used for training HANNA, and the g^E for multi-component mixtures is found by a geometric projection of the g^E of all constituent binary subsystems. In future work, new projection strategies could be developed for this purpose. Furthermore, it could be considered to include ternary data in the fitting process. This has a bad reputation for parameterizing physical g^E -models, but it could be worthwhile to test the option for hybrid models like HANNA. Even the introduction of ternary parameters could be considered.

Molecular embeddings. HANNA currently uses the pre-trained transformer model ChemBERTa-2 [30] to obtain the molecular embeddings from SMILES strings. ChemBERTa-2 was trained on a wide range of basic chemical data [30] and could be fine-tuned for the present application; however, this would largely increase the computational effort of the training without guaranteeing better results. Furthermore, as described above, we have observed minor deficiencies that are likely associated with issues of ChemBERTa-2 and may be resolved by a workaround within ChemBERTa-2, without the need for a complete revision. Another option would be to provide different molecular embeddings, e.g., based on the SELFormer [41] that uses SELFIES [42] instead of SMILES or even use learnable embeddings from a graph neural network [43].

Last but not least, we look forward to user feedback, which we will gladly use to further improve HANNA in ways we may not have anticipated yet.

4 Methods

4.1 HANNA architecture

Algorithm 1 explains the forward pass of the HANNA architecture, starting with the molecular embeddings, the temperature, and the composition of an arbitrary N -component mixture of interest as input and providing predictions for the molar excess Gibbs energy of the mixture and the activity coefficients of the N components in the mixture as output.

The input of HANNA contains the numerical molecular embeddings e_i of the N components that make up the mixture to be modeled, summarized in $\mathbf{E} = [e_1, \dots, e_N]$, which are calculated individually with the transformer-based model ChemBERTa-2 from the respective component’s SMILES (canonized with RDKit [45]). We use the ‘77M-MTR’ variant of ChemBERTa-2 from Hugging Face [40] with a slightly corrected tokenizer [28]. Additionally, HANNA requires the temperature T and the mole fractions x_1, \dots, x_{N-1} of $N - 1$ components as input. The HANNA architecture comprises three feed-forward neural networks (FFNN), namely, the `Embedding_Network`, the `Mixture_Network`, and the `Property_Network`. The `Embedding_Network` consists of one layer, while the other two networks consist of two layers. In all cases, we use the Sigmoid Linear Unit (SiLU) activation function with PyTorch’s default settings.

All layers are modified linear layers with 96 nodes (except for the input layer of the `Mixture_Network`, which consists of 98 nodes as the temperature and the projected mole fraction of the respective component are concatenated to the output of the `Embedding_Network`) to which a Lipschitz regularization (cf. Section 4.4) is applied. HANNA computes the molar excess Gibbs energy for the N -component mixture of interest through a geometric projection from the binary subsystems [38, 39, 46, 47, 48]. For this purpose, the mole fractions of the N -component mixture are projected onto all $N(N - 1)/2$ binary subsystems (cf. loop starting in step 6 of Algorithm 1). In this work, we use the Muggianu projection [31], which, unlike other projection methods, does not exhibit singular points at infinite dilution [49, 50]. The projected mole fractions X_i^{ij} and X_j^{ij} in the binary subsystem i - j are given by:

$$X_i^{(ij)} = \frac{1 + \tilde{x}_i - \tilde{x}_j}{2} \quad \text{and} \quad X_j^{(ij)} = \frac{1 + \tilde{x}_j - \tilde{x}_i}{2}, \quad (1)$$

Algorithm 1 Forward pass of HANNA. The HANNA architecture is implemented in *PyTorch* [44].

Input: temperature T , mole fractions $\mathbf{x} = [x_1, \dots, x_{N-1}]$, molecular ChemBERTa-2 embeddings $\mathbf{E} = [e_1, \dots, e_N]$

- 1: $T^* = \text{Temperature_Scaler}(T)$, $e_i^* = \text{Embedding_Scaler}(e_i)$ ▷ Scale inputs, cf. Section 4.2
- 2: $x_N = 1 - \sum_{i=1}^{N-1} x_i$ ▷ Calculate x_N via summation condition
- 3: $\boldsymbol{\theta}_i = \text{Embedding_Network}(e_i^*)$ ▷ Refine molecular embeddings
- 4: $R_{ij} = \exp(-\gamma \|\boldsymbol{\theta}_i - \boldsymbol{\theta}_j\|^2)$ with $\gamma = 100$ ▷ Compute component similarity score
- 5: $\tilde{x}_i = \sum_{j=1}^N x_j R_{ij}$ ▷ Lump identical components together, cf. Eq. (2)
- 6: **for all** $1 \leq i < j \leq N$ **do** ▷ Loop over all $K = N(N-1)/2$ binary subsystems
- 7: $X_i^{(ij)} = \frac{1 + \tilde{x}_i - \tilde{x}_j}{2}$; $X_j^{(ij)} = \frac{1 + \tilde{x}_j - \tilde{x}_i}{2}$ ▷ Muggianu projection, cf. Eq. (1)
- 8: $\mathbf{c}_i^{(ij)} = [\boldsymbol{\theta}_i, X_i^{(ij)}, T^*]$; $\mathbf{c}_j^{(ij)} = [\boldsymbol{\theta}_j, X_j^{(ij)}, T^*]$
- 9: $\boldsymbol{\alpha}_i^{(ij)} = \text{Mixture_Network}(\mathbf{c}_i^{(ij)})$; $\boldsymbol{\alpha}_j^{(ij)} = \text{Mixture_Network}(\mathbf{c}_j^{(ij)})$
- 10: $\phi_{ij} = \text{Property_Network}(\boldsymbol{\alpha}_i^{(ij)} + \boldsymbol{\alpha}_j^{(ij)})$ ▷ Compute binary interactions
- 11: $q_{ij} = \phi_{ij}(1 - R_{ij})$ ▷ Enforce consistency for pure components
- 12: $\frac{g^E}{RT} = \sum_{i=1}^{N-1} \sum_{j=i+1}^N x_i x_j q_{ij}$ ▷ Compute g^E as weighted sum over all binary interactions, cf. Eq. (3)
- 13: $\ln \gamma_i = \frac{g^E}{RT} + \frac{\partial}{\partial x_i} \left(\frac{g^E}{RT} \right) - \sum_{j=1}^{N-1} x_j \frac{\partial}{\partial x_j} \left(\frac{g^E}{RT} \right)$ ▷ Compute activity coefficients for components $i = 1, \dots, N-1$
- 14: $\ln \gamma_N = \frac{g^E}{RT} - \sum_{j=1}^{N-1} x_j \frac{\partial}{\partial x_j} \left(\frac{g^E}{RT} \right)$ ▷ Compute activity coefficient for component N
- 15: **return** $(\ln \gamma = [\ln \gamma_1, \dots, \ln \gamma_N], \frac{g^E}{RT})$

whereby \tilde{x}_i and \tilde{x}_j are the corrected mole fractions of component i and j respectively (cf. below). The projection strictly fulfills the summation condition in each binary subsystem, i.e., $X_i^{(ij)} + X_j^{(ij)} = 1$. Furthermore, if a binary mixture is studied, the projected mole fractions reduce to the corrected mole fractions, i.e., $X_i^{(ij)} = \tilde{x}_i$ and $X_j^{(ij)} = \tilde{x}_j$, ensuring a consistent transition of the HANNA predictions going from binary to a multi-component mixture. In contrast to the original publication [31], we correct the original mole fractions x_i in the N -component mixture before the projection as follows (cf. step 4 and 5 in Algorithm 1):

$$\tilde{x}_i = \sum_{j=1}^N x_j R_{ij} \quad \text{with} \quad R_{ij} \in [0, 1] \quad (2)$$

With this correction, we lump identical components, indicated by a component similarity score $R_{ij} = 1$, into a single component, thereby ensuring that, e.g., for a mixture of three components A, B, and C, where B is identical to C, the exact same results are obtained as for the binary mixture of A and B (when accounting for the lumped mole fractions). To compute the component similarity score R_{ij} , we apply the radial basis function (RBF) on pairs of the refined molecular embeddings. By setting the hyperparameter γ of the RBF to the high value of 100, we ensure that only extremely similar components result in a similarity score of $R_{ij} = 1$, so only components that we consider truly identical are lumped together.

Finally, the molar excess Gibbs energy g^E of the N -component mixture is calculated as follows [39]:

$$\frac{g^E}{RT} = \frac{1}{RT} \sum_{i=1}^{N-1} \sum_{j=i+1}^N \frac{x_i x_j}{X_i^{(ij)} X_j^{(ij)}} g_{ij}^E(X_i^{(ij)}, X_j^{(ij)}) = \sum_{i=1}^{N-1} \sum_{j=i+1}^N x_i x_j q_{ij}(X_i^{(ij)}, X_j^{(ij)}), \quad (3)$$

where g_{ij}^E is the molar excess Gibbs energy of the binary subsystem i - j and q_{ij} is the learned binary interaction between component i and j in the respective binary subsystem. q_{ij} is calculated using a deep set architecture [51] including a summation aggregation (cf. step 10 in Algorithm 1) to ensure the permutation invariance of the predicted molar excess Gibbs energy, i.e., to ensure that the order of the components in the input of HANNA does not influence its results. For technical reasons, namely, to prevent divisions by zero in Eq. (3) if one of the projected mole fractions approaches zero,

we directly predict the binary interaction term q_{ij} with HANNA for each binary subsystem in the projected space (cf. step 11 in Algorithm 1). Here, again, the component similarity score R_{ij} is used, ensuring physically sound predictions by enforcing $q_{ij} = 0$ and, ultimately, $g_{ij}^E = 0$ for identical components i and j . Using the Autograd functionality of *PyTorch*, the activity coefficients for all N components are finally derived from g^E of the N -component mixture (cf. steps 13 and 14 in Algorithm 1), ensuring strict Gibbs-Duhem consistency [52].

4.2 Data

The experimental data used to train and evaluate HANNA in this work were taken from the Dortmund Data Bank (DDB) [35]. Data points labeled as poor quality by internal criteria of the DDB were excluded. Furthermore, only components for which a canonical SMILES string could be generated with RDKit [45] using mol-files from the DDB were considered.

Vapor-liquid equilibrium. Only VLE data points in the DDB [35] that contain all information on temperature, pressure, as well as liquid and vapor phase compositions were considered. From these data, activity coefficients for all components i were calculated with the extended Raoult’s law:

$$\gamma_i = \frac{p y_i}{p_i^s x_i}, \quad (4)$$

where γ_i is the activity coefficient of component i normalized according to Raoult’s law in the mixture, x_i and y_i are the mole fractions of component i in the liquid and vapor phase in VLE, respectively, p denotes the total pressure, and p_i^s is the pure-component vapor pressure of i at the same temperature as the VLE data. The pure-component vapor pressures were computed using the Antoine equation with coefficients from the DDB [35]. By using the extended Raoult’s law, we assumed that the vapor phase can be treated as a mixture of ideal gases and that the pressure dependence of the chemical potential in the liquid phase can be neglected. To justify these assumptions, all VLE data points with pressures higher than 10 bar were excluded.

Activity coefficients at infinite dilution. Activity coefficients at infinite dilution γ_i^∞ normalized according to Raoult’s law, called ‘ACI’ throughout this work, were considered for binary and ternary mixtures. For binary mixtures, i.e., with pure solvents, these data could be used directly. For the activity coefficients at infinite dilution in mixed solvents, we observed several errors in the DDB, mostly interchanged solvent labels, so that these data had to be curated prior to use. Our detailed data curation protocol is described in Section Data curation of activity coefficients at infinite dilution in mixed solvents in the Supporting Information.

Liquid-liquid equilibrium. The LLE data in the DDB contains information on the temperature T and the mole fractions in the two coexisting phases x_i' and x_i'' . Data for binary, ternary, and quaternary mixtures were considered. For the data for the binary mixtures, we defined the phase compositions such that x_1' is always the phase composition with the lower value, i.e., $x_1'' > x_1'$ always holds, which is important for training the surrogate solver, cf. Section 4.3. Because HANNA does not consider the pressure dependence of the excess Gibbs energy, we excluded all LLE data points with pressures above 100 bar.

Data overview. Tab. 1 gives an overview of the final data sets for binary, ternary, and quaternary mixtures.

Table 1: Overview of the final data sets used in this work. All data were taken from the DDB [35].

	Data set	Data points	Systems	Components
Binary	VLE	193 880	5593	1024
	ACI	124 967	30 904	2283
	LLE	18 429	2289	1314
Ternary	VLE	43 705	1164	380
	ACI	5630	343	98
	LLE	23 322	1922	696
Quaternary	VLE	3678	124	101
	LLE	4268	294	209

Data splitting and scaling. Following a cross-validation approach, we randomly split the data sets for binary mixtures system-wise into ten folds, each representing a mutually exclusive test set of 10 % of the binary systems. A stratified split strategy was employed, such that the ratio of VLE and ACI to LLE data is roughly equal for all folds. The remaining data (90 % of the systems) of each fold were again split system-wise into a training set (90 %) and a validation set (10 %). In the data splits, all types of data, i.e., VLE, ACI, and LLE data, for a particular system were put exclusively within a single set; for instance, if LLE data for a particular system were in the test set, all VLE and ACI data for this system were also in the test set. This strategy enabled the use of all available data as unseen test data for the evaluation of HANNA.

Furthermore, an additional data split was carried out, where 95 % of the binary systems were used in the training set and 5 % in the validation set (i.e., no test set was withheld). This split, denoted as 'full data split' in the following, was used to train the model that was subsequently evaluated on the data for ternary and quaternary mixtures and is also deployed as the 'final model' with this work.

The molecular embeddings from ChemBERTa-2, as well as the temperature, were scaled using the *scikit-learn* [53] `StandardScaler()`. Individual scalers were fitted to each training data set to prevent any information leakage.

4.3 Surrogate LLE Solver

From the binary VLE data points, activity coefficients can be calculated directly using the extended Raoult’s Law, cf. Eq. (4). Hence, the training of HANNA on these data is straightforward using a loss function for the predicted activity coefficients, cf. Section 4.4. In contrast, it is not possible to explicitly calculate activity coefficients from the binary experimental LLE data. Using HANNA, one could obtain phase compositions for a given mixture and state point using iterative solvers [36] and compare to experimental data. However, integrating iterative solvers into a deep learning framework is tedious because gradients are not easily trackable and, moreover, it would significantly slow down the training process. To overcome this, we developed a differentiable surrogate solver to estimate the binary LLE phase compositions resulting from the activity coefficients predicted by HANNA. This surrogate solver is realized by a feed-forward neural network that mimics the convex envelope method (CEM) [32, 33, 34] and maps a discretized graph of the scaled molar Gibbs energy of mixing $\Delta g_{\text{mix}}/RT$ onto the compositions of the two coexisting liquid phases x'_1 and x''_1 . During the training of HANNA, the surrogate solver allows the model to directly learn from experimental LLE data while maintaining full compatibility with gradient-based optimization. The architecture and training process of the surrogate solver are described in the following.

As input, the surrogate solver gets a vector of $\Delta g_{\text{mix}}/RT$ values calculated with HANNA at 101 uniformly spaced discrete compositions from $x_1 = 0$ to $x_1 = 1 \text{ mol mol}^{-1}$ at constant temperature T . The $\Delta g_{\text{mix}}/RT$ values from HANNA are then processed through three fully connected layers with a hidden size of 64, each followed by the Rectified Linear Unit (ReLU) activation function. The output layer yields two values that correspond to x'_1 and x''_1 (we always define x'_1 as the phase composition with the lower value, cf. Section 4.2), which are subsequently processed through a sigmoid function to constrain the mole fractions between 0 and 1. To align with the demand of thermodynamic consistency of the model, the surrogate solver must be permutation-equivariant with respect to the order of the molecules in the input, i.e., if the discretized Gibbs energy of mixing is given in reverse order, it must yield $1 - x''_1$ and $1 - x'_1$. To enforce this, upon calling the forward function of the surrogate solver with a discretized $\Delta g_{\text{mix}}/RT$ vector, the phase compositions are calculated twice, both from the original vector and the reversed vector. The two values obtained for x'_1 and x''_1 are then averaged. Besides guaranteeing permutation-equivariance, this procedure also prevents any bias in the order of the training data from negatively impacting the training.

The surrogate solver was trained only on synthetic data, namely, predictions of $\Delta g_{\text{mix}}/RT$ obtained with mod. UNIFAC. More specifically, for every experimental LLE data point in our data set within the mod. UNIFAC horizon, we calculated $\Delta g_{\text{mix}}/RT$ for the 101 discrete uniformly spaced compositions at the temperature of the respective data point with mod. UNIFAC. We then used the CEM to determine the corresponding phase compositions, which served as the training objective of our surrogate solver. If no phase split was found, the data point was dropped. We used the same system-wise split as for the experimental data (cf. Section 4.2) to split the synthetic surrogate solver data into training, validation, and test sets. This prevents information leakage through the surrogate solver when training HANNA. Detailed results of the surrogate solver training are provided in the Supporting Information, along with an example of its functionality given in Fig. S.1.

4.4 Training of HANNA

HANNA was trained by minimizing the total loss $\mathcal{L}_{\text{total}}$ defined as:

$$\mathcal{L}_{\text{total}} = \frac{1}{N_b} (\mathcal{L}_{\text{VLE}} + \mathcal{L}_{\text{ACI}} + w_{\text{LLE}} \cdot \mathcal{L}_{\text{LLE}} + w_{\text{Gibbs}} \cdot \mathcal{L}_{\text{Gibbs}} + w_{\text{Lips}} \cdot \mathcal{L}_{\text{Lips}}), \quad (5)$$

where N_b is the batch size, \mathcal{L}_{VLE} , \mathcal{L}_{ACI} , \mathcal{L}_{LLE} are the individual data losses, $\mathcal{L}_{\text{Gibbs}}$ is the Gibbs loss, $\mathcal{L}_{\text{Lips}}$ is the Lipschitz regularization, and w_{LLE} , w_{Gibbs} , w_{Lips} are the corresponding weight factors that were determined in a hyperparameter grid search, cf. Supporting Information for details.

Data Losses. In the individual data losses, we use the `SmoothL1Loss()` loss function from *PyTorch* [44], which is less sensitive to outliers than the mean squared error loss. The parameter β in the `SmoothL1Loss()` function, which controls the transition between the mean absolute and mean squared error, was empirically set for each data type individually.

\mathcal{L}_{VLE} penalizes the average deviation of the two logarithmic activity coefficients predicted with HANNA from the respective experimental values derived from the VLE data for the binary systems from the training set:

$$\mathcal{L}_{\text{VLE}} = \sum_k^{N_{\text{VLE}}} \text{SmoothL1Loss}([\ln \gamma_{1,\text{pred}}, \ln \gamma_{2,\text{pred}}], [\ln \gamma_{1,\text{exp}}, \ln \gamma_{2,\text{exp}}]) \quad \text{with} \quad \beta = 1.0 \quad (6)$$

where N_{VLE} is the number of VLE data points in the training batch.

Similarly, \mathcal{L}_{ACI} takes into account errors in the prediction of the activity coefficients at infinite dilution $\ln \gamma_i^\infty$ for the binary systems from the training set:

$$\mathcal{L}_{\text{ACI}} = \frac{1}{2} \sum_k^{N_{\text{ACI}}} \text{SmoothL1Loss}(\ln \gamma_{i,\text{pred}}^\infty, \ln \gamma_{i,\text{exp}}^\infty) \quad \text{with} \quad \beta = 2.0, \quad (7)$$

where N_{ACI} is the number of ACI data points in the batch. The factor $\frac{1}{2}$ takes into account that in \mathcal{L}_{ACI} , each data point for an activity coefficient individually contributes to the loss calculation, whereas in \mathcal{L}_{VLE} , the errors of *both* activity coefficients in a binary mixture are averaged before contributing to the loss.

\mathcal{L}_{LLE} denotes the loss between the LLE phase compositions in mole fractions predicted by HANNA and the experimental values in the batch obtained through

$$\mathcal{L}_{\text{LLE}} = \sum_k^{N_{\text{LLE}}} m_k \cdot \text{SmoothL1Loss}([x'_{1,\text{pred}}, x''_{1,\text{pred}}], [x'_{1,\text{exp}}, x''_{1,\text{exp}}]) \quad \text{with} \quad \beta = 0.35, \quad (8)$$

where N_{LLE} is the number of LLE data points in the batch and $m_k \in \{0, 1\}$ is a binary mask that indicates if the respective data point is considered or not (cf. below for details). To obtain the predicted phase compositions $x'_{1,\text{pred}}, x''_{1,\text{pred}}$ for a data point during training, the pre-trained surrogate solver (cf. Section 4.3) is provided with the discretized molar Gibbs energy of mixing curve for the respective system and temperature. Since the surrogate solver is only trained on positive samples (i.e., binary LLE mixtures at state points with a miscibility gap) and cannot identify systems without miscibility gap, it will also falsely predict a phase split for a Δg_{mix} that does not fulfill the necessary condition for a phase split, which states

$$\left(\frac{\partial^2 \Delta g_{\text{mix}}}{\partial x_1^2} \right)_{T,p} < 0, \quad (9)$$

i.e., the second derivative of Δg_{mix} is negative somewhere in the composition space. This is unphysical and could potentially negatively impact the training process. Therefore, during the training, we account for the LLE loss of binary systems *only* if the necessary condition in Eq. (9) is true for at least one discretized composition; this is reflected in Eq. (8) through the binary mask m_k , where $m_k = 1$ for data points that exhibit an LLE and $m_k = 0$ for those that do not. The required second derivatives of Δg_{mix} were calculated by automatic differentiation.

Gibbs Loss. The \mathcal{L}_{LLE} described above alone does not penalize false negative LLE predictions. If HANNA fails to predict a liquid-liquid phase split, the necessary condition in Eq. (9) is not fulfilled and the binary mask is $m_k = 0$, cf. Eq. 8. To provide a learning incentive towards a correct detection of these phase splits, the additional loss term $\mathcal{L}_{\text{Gibbs}}$ was introduced:

$$\mathcal{L}_{\text{Gibbs}} = \sum_k^{N_{\text{LLE}}} \max \left(0, \min_d S_k(T_k, x_{1,d}) \right) \quad (10)$$

Here,

$$S_k(T_k, x_{1,d}) = \frac{1}{RT_k} \left(\frac{\partial^2 \Delta g_{\text{mix}}(T_k, x_{1,d})}{\partial x_1^2} \right)_T \quad (11)$$

is the second derivative of the molar Gibbs energy of mixing for data point k from the LLE training set evaluated at the composition d on the discretized grid of Δg_{mix} . Eq. 10 identifies the minimum of the second derivative of Δg_{mix} within the discretized composition space for each LLE training data point. If this minimum is negative, a miscibility gap is predicted by the model (cf. Eq. (9)) and the Gibbs loss is zero[‡]. On the other hand, if the minimum is positive, the miscibility gap is not identified by HANNA, and, consequently, the model is penalized by adding the respective value of S_k to the total loss.

Lipschitz Regularization. Besides the data losses and the Gibbs loss, $\mathcal{L}_{\text{Lips}}$ is included in the total loss function as a Lipschitz regularization term, controlling the Lipschitz constant of HANNA. Generally, the Lipschitz constant ($c \geq 0$) in the 2-norm is defined as

$$\|f(x_1) - f(x_0)\|_2 \leq c\|x_1 - x_0\|_2 \quad (12)$$

and provides an upper bound for the change of a function from $f(x_0)$ to $f(x_1)$ by changing the function input from x_0 to x_1 ; it is, therefore, a proxy for the smoothness of a function. For fully connected neural networks with L layers, a loose upper bound

$$c = \prod_{l=1}^L c_l = \prod_{l=1}^L \|\mathbf{W}_l\|_2 = \prod_{l=1}^L \sigma_{\max}(\mathbf{W}_l) \quad (13)$$

is obtained by the product of the spectral norms $\|\mathbf{W}_l\|_2$ of the weight matrices of each layer l , if the Lipschitz constants of the activation functions are neglected [54]. For HANNA, the influence of the summation of the two mixture embeddings (cf. step 10 in Algorithm 1) on the total Lipschitz constant is also neglected, since it does not contain any learnable parameters. The spectral 2-norm $\|\mathbf{W}_l\|_2$, in turn, equals the maximum singular value $\sigma_{\max}(\mathbf{W}_l)$ of the weight matrix \mathbf{W}_l . [55]

Following the approach from Ref. [54], all networks of HANNA are realized as modified linear layers with learnable Lipschitz constants c_l^* . In these layers, the raw weight matrices \mathbf{W}_{raw} are first normalized using the maximum singular value $\sigma_{\max}(\mathbf{W}_{l,\text{raw}})$ (such that their Lipschitz constant equals one) and then scaled using the learnable Lipschitz constants :

$$\mathbf{W}_{l,\text{scaled}} = \frac{\mathbf{W}_{l,\text{raw}}}{\sigma_{\max}(\mathbf{W}_{l,\text{raw}})} \cdot \text{softplus}(c_l^*) \quad (14)$$

These scaled weight matrices are then used in the forward function of the modified layers as a drop-in replacement of the raw weight matrices. For computational efficiency, we approximate $\sigma_{\max}(\mathbf{W}_{l,\text{raw}})$ with a power iteration method using two iterations [55]. The Lipschitz regularization term used in the total loss function, cf. Eq. (5), is calculated via [54]

$$\mathcal{L}_{\text{Lips}} = \prod_{l=1}^L \text{softplus}(c_l^*) \quad (15)$$

by multiplying the total Lipschitz constants of the networks (given by the product of the layer-wise learned constants of all L layers in the model and ignoring other factors, cf. above). The softplus transformation of c_l^* avoids infeasible negative Lipschitz constants [54]. The hyperparameter w_{Lips} , cf. Eq. (5), can be used to control the learnable Lipschitz constants of the network, i.e., higher values of w_{Lips} lead to lower Lipschitz constants and vice versa. For the model variants in the grid search with $w_{\text{Lips}} = 0$, we employed a L2-regularization instead to prevent exploding parameters.

Training Details The HANNA models for this work were trained for 200 epochs using a batch size of 512, the AdamW optimizer and the OneCycleLR scheduler ($\text{max_lr}=0.01$) from PyTorch. The best epoch was selected based on the weighted sum of the data losses ($\mathcal{L}_{\text{VLE}}, \mathcal{L}_{\text{ACI}}, \mathcal{L}_{\text{LLE}}$) on the respective validation set, whereby only models that were trained for at least 50 epochs were considered.

After determining the optimal hyperparameters through a grid search (cf. Section Grid Search in the Supporting Information), we trained an ensemble of ten models (starting from different weight initializations) for each data fold (cf. Section 4.2). Additionally, we trained such an ensemble for the full data split; this model is also published as final model along this work.

4.5 Evaluation of HANNA

For the systematic evaluation of HANNA and the benchmark models, absolute deviations ϵ between the predicted and the experimental values for each data point in the considered test set were calculated.

[‡]Note that in this case ($m_k = 1$) the deviation to experimental data is accounted for by \mathcal{L}_{LLE} .

For each VLE data point, a mean absolute error in the logarithmic activity coefficients of all components i in the test mixture at the respective temperature T and composition x was calculated:

$$\epsilon_{\text{VLE}} = \frac{1}{N} \sum_{i=1}^N |\ln \gamma_i^{\text{pred}} - \ln \gamma_i^{\text{exp}}| \quad (16)$$

Here, N is the number of components in the mixture ($N = 2$ for binary, $N = 3$ for ternary, $N = 4$ for quaternary mixtures).

For each ACI data point, i.e., activity coefficients at infinite dilution in pure or in mixed solvents, only the logarithmic activity coefficient of the infinitely diluted solute i in the solvent(s) was considered for error calculation:

$$\epsilon_{\text{ACI}} = |\ln \gamma_i^{\text{pred},\infty} - \ln \gamma_i^{\text{exp},\infty}| \quad (17)$$

For each LLE data point, the mean absolute errors of the phase compositions in mole fractions x'_i and x''_i of all components i in the mixture were calculated:

$$\epsilon_{\text{LLE}} = \frac{1}{2N} \sum_{i=1}^N |x'_{i,\text{pred}} - x'_{i,\text{exp}}| + |x''_{i,\text{pred}} - x''_{i,\text{exp}}| \quad (18)$$

From the data point-wise error scores described above, also system-wise mean absolute error MAE_{sys} scores were calculated by averaging over all data points (at all temperatures and compositions) for each binary, ternary, or quaternary system. The system-wise error scores are favorable as they are independent of the number of available data points for a particular system and do not over-emphasize systems with many data points, such as (ethanol + water). Therefore, they are more suitable to evaluate the performance of the models to generalize over unseen systems and components.

The HANNA predictions shown in the evaluation of this work were obtained using ensembles of ten individual models. For the binary data, we used the ten independently trained ensembles and evaluated them on their respective test set. For the multi-component data, the final model, i.e., the ensemble trained on the full data split, was used.

Supporting Information

The Supporting Information contains additional information on the data curation, the surrogate solver, and the grid search. Moreover, it provides additional comparisons of HANNA to the other benchmark models (mod. UNIFAC 2.0 and UNIFAC-LLE) and the results for quaternary data. Furthermore, an evaluation of the quality of the employed geometric projection method is shown.

Declaration of Competing Interests

The authors declare that they have no known competing financial interests.

Acknowledgments

We gratefully acknowledge financial support by the Carl Zeiss Foundation in the frame of the project 'Process Engineering 4.0' and by DFG in the frame of the Priority Program SPP2363 'Molecular Machine Learning' (grant number 497201843). Furthermore, FJ gratefully acknowledges financial support by DFG in the frame of the Emmy-Noether program (grant number 528649696).

References

- [1] Henri Renon and J. M. Prausnitz. Local compositions in thermodynamic excess functions for liquid mixtures. *AIChE Journal*, 14(1):135–144, January 1968.
- [2] Denis S. Abrams and John M. Prausnitz. Statistical thermodynamics of liquid mixtures: A new expression for the excess gibbs energy of partly or completely miscible systems. *AIChE Journal*, 21(1):116–128, January 1975.
- [3] Jürgen Rarey. Extended flexibility for g^E models and simultaneous description of vapor-liquid equilibrium and liquid-liquid equilibrium using a nonlinear transformation of the concentration dependence. *Industrial & Engineering Chemistry Research*, 44(19):7600–7608, August 2005.

- [4] A. Marcilla, M.M. Olaya, and J.A. Reyes-Labarta. Simultaneous vll data correlation for ternary systems: Modification of the nrtl equation for improved calculations. *Fluid Phase Equilibria*, 426:47–55, October 2016.
- [5] Aage Fredenslund, Russell L. Jones, and John M. Prausnitz. Group-contribution estimation of activity coefficients in nonideal liquid mixtures. *AIChE Journal*, 21(6):1086–1099, November 1975.
- [6] Roland Wittig, Jürgen Lohmann, and Jürgen Gmehling. Vapor-liquid equilibria by unifac group contribution. 6. revision and extension. *Industrial & Engineering Chemistry Research*, 42(1):183–188, November 2002.
- [7] Ulrich Weidlich and Jürgen Gmehling. A modified unifac model. 1. prediction of vle, he, and γ_{∞} . *Industrial & Engineering Chemistry Research*, 26(7):1372–1381, July 1987.
- [8] Dana Constantinescu and Jürgen Gmehling. Further development of modified unifac (dortmund): Revision and extension 6. *Journal of Chemical & Engineering Data*, 61(8):2738–2748, May 2016.
- [9] Thomas Magnussen, Peter Rasmussen, and Aage Fredenslund. Unifac parameter table for prediction of liquid-liquid equilibria. *Industrial & Engineering Chemistry Process Design and Development*, 20(2):331–339, April 1981.
- [10] Zhigang Lei, Jiguo Zhang, Qunsheng Li, and Biaohua Chen. Unifac model for ionic liquids. *Industrial & Engineering Chemistry Research*, 48(5):2697–2704, January 2009.
- [11] Ruisong Zhu, Hongwei Kang, Qinghua Liu, Minghao Song, Chengmin Gui, Guoxuan Li, and Zhigang Lei. Unifac model for ionic liquids: 3. revision and extension. *Industrial & Engineering Chemistry Research*, 63(3):1670–1679, January 2024.
- [12] Niklas Schmitz, Anne Friebel, Erik von Harbou, Jakob Burger, and Hans Hasse. Liquid-liquid equilibrium in binary and ternary mixtures containing formaldehyde, water, methanol, methylal, and poly(oxymethylene) dimethyl ethers. *Fluid Phase Equilibria*, 425:127–135, October 2016.
- [13] Niklas Schmitz, Christian F. Breitzkreuz, Eckhard Ströfer, Jakob Burger, and Hans Hasse. Vapor-liquid equilibrium and distillation of mixtures containing formaldehyde and poly(oxymethylene) dimethyl ethers. *Chemical Engineering and Processing - Process Intensification*, 131:116–124, September 2018.
- [14] A. Klamt and G. Schüürmann. Cosmo: a new approach to dielectric screening in solvents with explicit expressions for the screening energy and its gradient. *J. Chem. Soc., Perkin Trans. 2*, (5):799–805, 1993.
- [15] Andreas Klamt. Conductor-like screening model for real solvents: A new approach to the quantitative calculation of solvation phenomena. *The Journal of Physical Chemistry*, 99(7):2224–2235, February 1995.
- [16] Shiang-Tai Lin and Stanley I. Sandler. A priori phase equilibrium prediction from a segment contribution solvation model. *Industrial & Engineering Chemistry Research*, 41(5):899–913, December 2001.
- [17] Hans Grensemann and Jürgen Gmehling. Performance of a conductor-like screening model for real solvents model in comparison to classical group contribution methods. *Industrial & Engineering Chemistry Research*, 44(5):1610–1624, February 2005.
- [18] Thomas Gerlach, Simon Müller, Andrés González de Castilla, and Irina Smirnova. An open source cosmo-rs implementation and parameterization supporting the efficient implementation of multiple segment descriptors. *Fluid Phase Equilibria*, 560:113472, September 2022.
- [19] Shu Wang, John M. Stubbs, J. Ilja Siepmann, and Stanley I. Sandler. Effects of conformational distributions on sigma profiles in cosmo theories. *The Journal of Physical Chemistry A*, 109(49):11285–11294, November 2005.
- [20] Tiancheng Mu, Jürgen Rarey, and Jürgen Gmehling. Performance of cosmo-rs with sigma profiles from different model chemistries. *Industrial & Engineering Chemistry Research*, 46(20):6612–6629, September 2007.
- [21] Robert Franke and Bernd Hannebauer. On the influence of basis sets and quantum chemical methods on the prediction accuracy of cosmo-rs. *Physical Chemistry Chemical Physics*, 13(48):21344, 2011.
- [22] Robin Fingerhut, Wei-Lin Chen, Andre Schedemann, Wilfried Cordes, Jürgen Rarey, Chieh-Ming Hsieh, Jadran Vrabec, and Shiang-Tai Lin. Comprehensive assessment of cosmo-sac models for predictions of fluid-phase equilibria. *Industrial & Engineering Chemistry Research*, 56(35):9868–9884, August 2017.
- [23] Zhimin Xue, Tiancheng Mu, and Jürgen Gmehling. Comparison of the a priori cosmo-rs models and group contribution methods: Original unifac, modified unifac(do), and modified unifac(do) consortium. *Industrial & Engineering Chemistry Research*, 51(36):11809–11817, August 2012.
- [24] Fabian Jirasek, Robert Bamler, Sophie Fellenz, Michael Bortz, Marius Kloft, Stephan Mandt, and Hans Hasse. Making thermodynamic models of mixtures predictive by machine learning: matrix completion of pair interactions. *Chemical Science*, 13(17):4854–4862, 2022.

- [25] Benedikt Winter, Clemens Winter, Timm Esper, Johannes Schilling, and André Bardow. Spt-nrtl: A physics-guided machine learning model to predict thermodynamically consistent activity coefficients. *Fluid Phase Equilibria*, 568:113731, May 2023.
- [26] Nicolas Hayer, Thorsten Wendel, Stephan Mandt, Hans Hasse, and Fabian Jirasek. Advancing thermodynamic group-contribution methods by machine learning: Unifac 2.0. *Chemical Engineering Journal*, 504:158667, January 2025.
- [27] Nicolas Hayer, Hans Hasse, and Fabian Jirasek. Modified unifac 2.0-a group-contribution method completed with machine learning. *Industrial & Engineering Chemistry Research*, 64(20):10304–10313, May 2025.
- [28] Thomas Specht, Mayank Nagda, Sophie Fellenz, Stephan Mandt, Hans Hasse, and Fabian Jirasek. Hanna: hard-constraint neural network for consistent activity coefficient prediction. *Chemical Science*, 15(47):19777–19786, 2024.
- [29] David Weininger. Smiles, a chemical language and information system. 1. introduction to methodology and encoding rules. *Journal of Chemical Information and Computer Sciences*, 28(1):31–36, February 1988.
- [30] Walid Ahmad, Elana Simon, Seyone Chithrananda, Gabriel Grand, and Bharath Ramsundar. Chemberta-2: Towards chemical foundation models. arXiv:2209.01712, 2022.
- [31] Yves-Marie Muggianu, Michèle Gambino, and Jean-Pierre Bros. Enthalpies de formation des alliages liquides bismuth-étain-gallium à 723 k. choix d’une représentation analytique des grandeurs d’excès intégrales et partielles de mélange. *Journal de Chimie Physique*, 72:83–88, 1975.
- [32] O. Ryll, S. Blagov, and H. Hasse. Convex envelope method for the determination of fluid phase diagrams. *Fluid Phase Equilibria*, 324:108–116, June 2012.
- [33] Quirin Göttl, Jonathan Pirnay, Dominik G. Grimm, and Jakob Burger. Convex envelope method for determining liquid multi-phase equilibria in systems with arbitrary number of components. *Computers & Chemical Engineering*, 177:108321, September 2023.
- [34] Quirin Göttl, Natalie Rosen, and Jakob Burger. Convex envelope method for t, p flash calculations for mixtures with an arbitrary number of components and arbitrary aggregate states. *Computers & Chemical Engineering*, page 109326, August 2025.
- [35] Dortmund data bank. www.ddbst.com, 2024.
- [36] Jürgen Gmehling, Michael Kleiber, Bärbel Kolbe, and Jürgen Rarey. *Chemical thermodynamics for process simulation*. John Wiley & Sons, 2 edition, 2019.
- [37] Andreas Klamt, Gerard J. P. Krooshof, and Ross Taylor. Cosmospace: Alternative to conventional activity-coefficient models. *AIChE Journal*, 48(10):2332–2349, October 2002.
- [38] Tianhua Ju, Xueyong Ding, Weiliang Chen, Xinlin Yan, and Yue Dong. A new perspective on geometric thermodynamic models. *Journal of Phase Equilibria and Diffusion*, 40(5):715–724, October 2019.
- [39] Tianhua Ju, Zhenlin Huang, Xueyong Ding, Xinlin Yan, and Changzong Liao. A unified extrapolation thermodynamic model for multicomponent solutions based on binary data. *Thermochimica Acta*, 740:179824, October 2024.
- [40] Huggingface chemberta-2 model. <https://huggingface.co/DeepChem/ChemBERTa-77M-MTR>, Last accessed: 08.07.2025.
- [41] Atakan Yüksel, Erva Ulusoy, Atabey Ünlü, and Tunca Doğan. Selfformer: molecular representation learning via selfies language models. *Machine Learning: Science and Technology*, 4(2):025035, June 2023.
- [42] Mario Krenn, Florian Häse, AkshatKumar Nigam, Pascal Friederich, and Alan Aspuru-Guzik. Self-referencing embedded strings (selfies): A 100 *Machine Learning: Science and Technology*, 1(4):045024, October 2020.
- [43] David Duvenaud, Dougal Maclaurin, Jorge Aguilera-Iparraguirre, Rafael Gómez-Bombarelli, Timothy Hirzel, Alán Aspuru-Guzik, and Ryan P. Adams. Convolutional networks on graphs for learning molecular fingerprints. arXiv:1509.09292, 2015.
- [44] Adam Paszke, Sam Gross, Francisco Massa, Adam Lerer, James Bradbury, Gregory Chanan, Trevor Killeen, Zeming Lin, Natalia Gimelshein, Luca Antiga, Alban Desmaison, Andreas Köpf, Edward Yang, Zach DeVito, Martin Raison, Alykhan Tejani, Sasank Chilamkurthy, Benoit Steiner, Lu Fang, Junjie Bai, and Soumith Chintala. Pytorch: An imperative style, high-performance deep learning library. arXiv:1912.01703, 2019.
- [45] RDKit: Open-source cheminformatics. <http://www.rdkit.org>. Version: 2023.03.1.
- [46] Arthur D. Pelton. A general “geometric” thermodynamic model for multicomponent solutions. *Calphad*, 25(2):319–328, June 2001.

- [47] Qun Luo, Cong Zhai, Dongke Sun, Wei Chen, and Qian Li. Interpolation and extrapolation with the calphad method. *Journal of Materials Science & Technology*, 35(9):2115–2120, September 2019.
- [48] Patrice Chartrand and Arthur D. Pelton. On the choice of “geometric” thermodynamic models. *Journal of Phase Equilibria*, 21(2):141–147, March 2000.
- [49] Weiji Cheng and Jibamitra Ganguly. Some aspects of multicomponent excess free energy models with subregular binaries. *Geochimica et Cosmochimica Acta*, 58(18):3763–3767, September 1994.
- [50] Reed A. Howald and Bimalendu N. Roy. Muggianu and toop-muggianu interpolations comment on a comment by I. Kaufman (calphad, 225 (1981)) on brynstad’s paper (calphad, , 103 (1981)). *Calphad*, 6(1):57–63, January 1982.
- [51] Manzil Zaheer, Satwik Kottur, Siamak Ravanbakhsh, Barnabas Poczos, Ruslan Salakhutdinov, and Alexander Smola. Deep sets. arXiv:1703.06114, 2017.
- [52] Ulrich K. Deiters and Thomas Kraska. *High-Pressure Fluid Phase Equilibria*. Elsevier Science & Technology Books, 2012.
- [53] F. Pedregosa, G. Varoquaux, A. Gramfort, V. Michel, B. Thirion, O. Grisel, M. Blondel, P. Prettenhofer, R. Weiss, V. Dubourg, J. Vanderplas, A. Passos, D. Cournapeau, M. Brucher, M. Perrot, and E. Duchesnay. Scikit-learn: machine learning in python. *Journal of Machine Learning Research*, 12:2825–2830, 2011.
- [54] Hsueh-Ti Derek Liu, Francis Williams, Alec Jacobson, Sanja Fidler, and Or Litany. Learning smooth neural functions via lipschitz regularization. arXiv:2202.08345, 2022.
- [55] Takeru Miyato, Toshiki Kataoka, Masanori Koyama, and Yuichi Yoshida. Spectral normalization for generative adversarial networks. arXiv:1802.05957, 2018.